G-C$_3$N$_4$/Ag@CoWO$_4$: A novel sunlight active ternary nanocomposite for potential photocatalytic degradation of rhodamine B dye

Hira Ashiq [a], Nimra Nadeem [a], Asim Mansha [b,**], Javed Iqbal [a], Muhammad Yaseen [c], Muhammad Zahid [a,*], Imran Shahid [d]

[a] *Department of Chemistry, University of Agriculture Faisalabad, Faisalabad, 38040, Pakistan*
[b] *Department of Chemistry, Govt. College University Faisalabad, Pakistan*
[c] *Department of Physics, University of Agriculture Faisalabad, Pakistan*
[d] *Environmental Science Centre, Qatar University, Doha, 2713, Qatar*

ARTICLE INFO

ABSTRACT

Present study reports the fabrication of novel sunlight active heterogeneous photocatalyst, i.e. Ag@g-C$_3$N$_4$/CoWO$_4$ for potential degradation of rhodamine B dye. The ternary nanocomposite was fabricated using thermal condensation of melamine to prepare g-C$_3$N$_4$ followed by coupling with silver doped cobalt tungstate (Ag@CoWO$_4$) using the hydrothermal method. The novel composite photocatalyst (Ag@g-C$_3$N$_4$/CoWO$_4$) along with pristine photocatalysts (g-C$_3$N$_4$ and Ag@CoWO$_4$) were well characterized in term of morphology (scanning electron microscopy), structure (Fourier Transformed Infrared spectroscopy), crystallinity (X-ray diffraction), and composition (energy dispersive X-ray). The energy band gaps of catalysts were calculated using UV–visible spectroscopic analysis (Tauc plot). The characterization analysis supports the successful assembly of Ag@CoWO$_4$ nanoparticles on the surface of g-C$_3$N$_4$ nanosheets with good crystallinity. The photocatalytic potential of novel catalysts was examined through the degradation of rhodamine B dye in water. The engineered heterojunction promotes photocatalytic activity and improves photo-generated charge separation. The results of the proposed research showed boosted sunlight active photocatalytic efficiency (97% in 120 min at pH 6) of novel composite against rhodamine B dye degradation. The kinetics of the reaction was determined using different models and RSM was used as a statistical tool for interaction and individual effects of influencing parameters. The numerical values of optimized parameters endorsed the results of RSM i.e. composite dose = 10mg/100 mL, H$_2$O$_2$ = 15 mM, and pH = 6.

1. Introduction

Water is essential for the existence of life and can be pondered most precious natural resources that must be treated, recycled, and conserved systematically for maintainable growth. The regulation of water pollution has become the leading challenge for researchers with its primary distress for the conservation and protection of natural reserves of water [1]. Nowadays, modern civilization and growing industries are producing discharge of dangerous chemicals into water bodies causing life hazards [2]. Textile dyes generate a heavy part of organic contaminants that result in serious environmental pollution as even small expulsion of dye may detrimentally affect marine and human life [3–6]. It is substantial to build an active scheme to remove tenacious organic

pollutants from wastewater. The photocatalysis consuming semiconductor stands the safe, cost-effective, green, and most influential technique for the effective degradation of dangerous organic contaminants [7].

Until now, several conventional procedures have been accustomed for the purification of water like reverse osmosis, sedimentation, coagulation, adsorption, and filtration, biological and chemical techniques [8–11]. The capacity of these therapeutic methods is not significant for the sanitization of water having a variety of contaminants like pharmaceuticals, pesticides, household chemicals, and organic solvents [12]. The development of ecological techniques to eliminate environmental noxious waste has become the primary concern of the current age while facing a tough period of energy shortage. Sunlight has been sponsored as

---

the ultimate power to solve the pollution dismissal and energy shortage with outstanding advantages including inexhaustible supply and environmentally friendly [13]. Among different sustainable procedures, semiconductor-assisted photocatalysis is deliberated as a most promising and alluring technique to directly consume sunlight for the resolution of environmental issues [14]. After the establishment of the photocatalytic splitting of water via TiO_2 centered electrodes, photocatalysis has obtained great consideration to degrade organic chemicals efficiently. This practice can result in overall organic contaminants degradation into CO_2, H_2O, and other harmless final products by consuming oxygen as an oxidant and so can maintain the previous deliberation for the protection of the environment [15]. In general, photocatalysis based on semiconductors are economic, renewable, clean, and safe technology, which aids reactions for different applications as, CO_2 reduction, water splitting, organic contaminants removal, bacterial disinfection, and selective production of organic complexes [16–18].

Since photocatalysis is pondered as a favorable technique to resolve the growing energy and environmental problems, semiconductors have enticed much attention as photocatalysts [10,16]. Numerous inorganic semiconductors based on metals like TiO_2 and ZnO had shown potential for the degradation of environmental pollutants but the central problem in consuming these photocatalysts is their failure to react towards visible light radiation. Contrarily, several other photocatalysts that respond to visible light like Bi_2WO_6, $BiVO_4$, $ZnFe_2O_4$, and g-C_3N_4 have also been revealed well [15]. Recently, profound consideration has been gained by carbon-containing compounds for their significant impact as components in admiration of different conservational applications [19]. For example the use of zeolite-based semiconductor photocatalysts [5,8,20], polyaniline based composite material [21], MWCNTs and carbon nanofiber photocatalysts [22,23], graphitic carbon nitride based composite materials [4–6,24], graphene oxide supported photocatalysts [10, 25–28], and doped semiconductor photocatalysts [29,30] have been used for enhanced photocatalytic degradation of various organic pollutants. The suitability of 0D, 1D, and 2D nanocarbon semiconductor composites has been specified by many scientists in perspective to their exceptional photocatalytic potential towards energy generation and in pollutant degradation [26,31].

Recently, several photocatalysts with significant potential in visible light were developed based on graphitic carbon nitride (g-C_3N_4). This semiconductor showed the obvious potential to be an auspicious photocatalyst with some captivating properties [32]. The g-C_3N_4 has revealed a markedly organized and tremendously stable polymeric structure among other important 2D carbon materials [33]. It is usually comprised of nitrogen and carbon. Its carbon-based structure permits its reactivity alteration with the least modification in its general composition [34]. It acts as a suitable photocatalyst active in visible light owing to its appropriate energy gap. It maintains outstanding properties of photocatalysis, like, harvesting sunlight, facile synthesis, photocatalysis, thermal and chemical stability, cheapness, and appropriateness towards redox potential to efficiently catalyze reactions [35]. Though, g-C_3N_4 does not ensure adequate activity owed to fast rejoining of (e^-/h^+) pairs, poor visible-light consumption, and small surface area [36]. Henceforth, some methodologies have been established to increase the photocatalytic potential of pure g-C_3N_4 including metallic and nonmetallic doping, modifying its morphology, preparation of mesoporous structures, assimilating with other semiconductors, and depositing particles of noble metals [37]. The higher charge mobility and electrical conductivity have been identified for g-C_3N_4 doped with metal [38]. The manufacture of heterojunction assembly among semiconductors may significantly increase the photocatalytic potential of novel compounds by enhancing the charge separation capacity and extending the light-harvesting range [16].

Lately, certain photocatalysts were offered with metal tungstates [39]. Among these semiconductors, with a 2.80 eV band gap, $CoWO_4$ has an average energy gap semiconductor. The $CoWO_4$ has been

employed in photocatalytic procedures alone and combined along with other compounds [37]. The conduction band (CB) and valance band (VB) energies of Cobalt tungstate are $+0.35$ and $+3.15$ eV. Hereafter, it appears that by the incorporation of $CoWO_4$ with g-C_3N_4, the photocatalytic potential of the synthesized g-C_3N_4 centered photocatalyst might be improved [32]. Recently, a tungstate semiconductor with bivalent metal ($M^{+2}WO_4$) has attained considerable attention due to its extraordinary thermal and chemical stability. Graphitic carbon nitride coupled with metal tungstates has better activity in visible light [40]. A nanocomposite ($FeWO_4$/g-C_3N_4) was synthesized that had the great photocatalytic potential for treating a dye (rhodamine B) [41]. Most recently, g-C_3N_4/$CdWO_4$ heterojunction photocatalyst has also been established for rhodamine and minocycline dye degradation [42]. A $CoWO_4$ composite is a potential material amongst various metal-tungstate compounds, for practical applications due to its great versatility [43]. Particularly g-C_3N_4 interceded photocatalyst has been commonly used with metal oxide compounds for the progressive oxidation process as an advanced catalyst [44]. Furthermore, the cobalt tungstate ($CoWO_4$) possessing higher electrical conductivity 10^{-7}–10^{-3} Scm^{-2} and possible redox (Co^{2+}/Co^{3+}) couple states, exhibits outstanding catalytic efficiency as equated to pristine or mixed metal oxide compounds. The introduction of tungstate atoms may considerably increase conductivity comparable to pure cobalt oxide [45]. Doping the cobalt tungstate with Nobel metal (Ag) is expected to improve the optical and well as photocatalytic properties of pristine cobalt tungstate.

In the present work, a novel heterogenous ternary photocatalyst g-C_3N_4/Ag@$CoWO_4$ was fabricated using a facile hydrothermal approach and used for the oxidative photocatalytic degradation of rhodamine B (RhB) dye. Owing to the fascinating light response of nanocomposite, the sunlight was selected as an excitation source for photocatalysis. The characterization of the prepared photocatalysts was done using different analytical techniques (e.g. X-ray diffraction (XRD), Fourier transform infrared (FTIR), and scanning electron microscopy–energy-dispersive X-ray (SEM–EDX). The intercalation of g-C_3N_4 with Ag@$CoWO_4$ was found as a novel and potent combination to increase the light absorption and providing superior photocatalytic properties. The dye degradation was monitored using UV–Vis spectrophotometer during experiments. Two kinetic models (1st and 2nd) were used for the determination of rate constant and reaction mechanism of the photocatalytic reaction. Central composite design (CCD) under response surface methodology (RSM) was used for statistical evaluation of mutual and independent effects of influencing parameters.

2. Materials and methods

2.1. Chemicals

All the chemicals and reagents were used as obtained. Melamine (>98%) and $AgNO_3$ (99.9%) were purchased from DAEJUNG. $Na_2WO_4·2H_2O$ (97%), $CoNO_3.6H_2O$ (>98%), NaOH (BioXtra, ≥ 98%), and HCl (35% w/w) were obtained from Sigma Aldrich., ethanol (95.6%) were purchased from UNI-CHEM. Distilled water was used throughout the experiments.

2.2. Synthesis

2.2.1. Synthesis of g-C_3N_4
The g-C_3N_4 was fabricated via a one-pot process by heating melamine (10g) for 2 h in a muffle furnace (heating rate 15 °C/min) at 550 °C. The ceramic crucible was cooled and yellowish g-C_3N_4 was obtained. The yellowish porous material was ground to powder by pestle and mortar [46].

2.2.2. Synthesis of $CoWO_4$
Cobalt tungstate was synthesized through a hydrothermal approach. For its preparation, 3.3 g $Co(NO_3)_2·6H_2O$ and 2.90g $Na_2WO_4·2H_2O$ were

mixed with 40 mL of distilled water. The unclear solution was stirred for 1 h and placed in the oven at 180 °C for 24 h in a stainless-steel autoclave reactor. The autoclave reactor was cooled at room temperature. The precipitates were separated and washed with distilled water and ethanol. The end product was dried at 60 °C. Lastly, the obtained cobalt tungstate was calcined for 2.0 h at 450 °C in a muffle furnace [47].

2.2.3. Synthesis of Ag@CoWO₄ nanoparticles

$AgNO_3$ aqueous solution (5 mL, 5 mol percent) was added to the solution of cobalt tungstate (0.2 g $CoWO_4$ powder/5 mL H_2O) under constant stirring. An aqueous solution of $NaBH_4$ (10 mL of 0.019 M) was added to the above mixture. Then the mixture was stirred vigorously for 30 min and kept at 30 °C for 4 h, the color of the solution was altered to gray. The final product was rinsed with distilled water and ethanol and the final sample was dried for 2 h at 60 °C [48].

2.2.4. Synthesis of g-C₃N₄/Ag@CoWO₄ nanocomposite

The ternary composite of g-C₃N₄/Ag@ CoWO₄ was prepared through the following procedure. The desired quantity of g-C₃N₄ and Ag@ CoWO₄ (1:1ratio) were combined and ground together for 15 min. Then the mixture was calcined for 4 h at 400 °C to obtain g-C₃N₄/Ag@ CoWO₄ nanocomposite photocatalyst [49]. A schematic representation for the synthesis process is presented in Fig. 1.

2.3. Characterization

The analytical methods used for the characterization of g-C₃N₄, Ag@CoWO₄, and g-C₃N₄/Ag@CoWO₄ photocatalysts were SEM associated with EDX (NANOSEM-EDX; FEI NOVA 450) for structural elucidation and elemental mapping of the photocatalysts. The crystalline structure was determined through powder XRD (Philips PANalytical Xpert pro DY 3805 XRD). To examine the different functional groups present in as-synthesized photocatalysts, FTIR (Agilent technologies) was used. The optical behavior was checked by the band gap energy (Tauc plot method) via a UV–visible spectrophotometer (CECIL 7200). The UV–visible spectrophotometer was also used to determine the photocatalytic degradation efficiency of synthesized photocatalysts.

2.4. Photocatalytic degradation experiment

The degradation efficiency of photocatalysts was estimated under ambient sunlight. The solar power meter (SM206) was used to measure the intensity of sunlight and brightness was measure using a Lux meter.

In a typical process for degradation test 100 mL of 10 ppm RhB was used in borosilicate glass beakers. The pH of solutions was maintained using 0.1 M NaOH and HCl solutions and catalyst was added. After that, the reaction mixture was kept in dark for 30 min under constant stirring (160 rpm) on an orbital shaker to attain the adsorption equilibrium and adsorption was checked using a spectrophotometer. Thereafter, oxidant was added, and solutions were placed under sunlight for oxidative photocatalysis. The average measured intensity of light was ~1200 W/m² while the brightness was measured in the range of 103,000 ± 2000 Lux. The samples were taken after successive intervals, the catalyst was separated, and absorbance was checked using a spectrophotometer at its $\lambda_{max} = 554$ nm. The % dye degradation was obtained with the help of formula given below [28]:

$$\text{Degradation} \ (\%) = \left(\frac{A_o - A_t}{A_o}\right) \times 100 \tag{1}$$

Other reaction parameters i.e. pH, catalyst dose, oxidant dose, and reaction time was monitored using a similar process.

3. Results and discussion

3.1. Characterization

3.1.1. FTIR analysis

The existence of functional groups and surface composition was studied by FTIR spectroscopy and obtained graphs are presented in Fig. 2. In the FTIR spectrum of pristine g-C₃N₄, the wide bands from 3000 cm⁻¹ to 3400 cm⁻¹ are representative of the N–H vibration [50]. The CN hetero-cycles bands were recorded at 1639 cm⁻¹, 1251 cm⁻¹, and 1575 cm⁻¹ [51]. The peaks at 808 cm⁻¹ are credited to the standard bending vibration of triazine [52]. The spectrum of Ag@CoWO₄ over the 400-4000 cm⁻¹ frequency range is depicted in Fig. 2. In the low
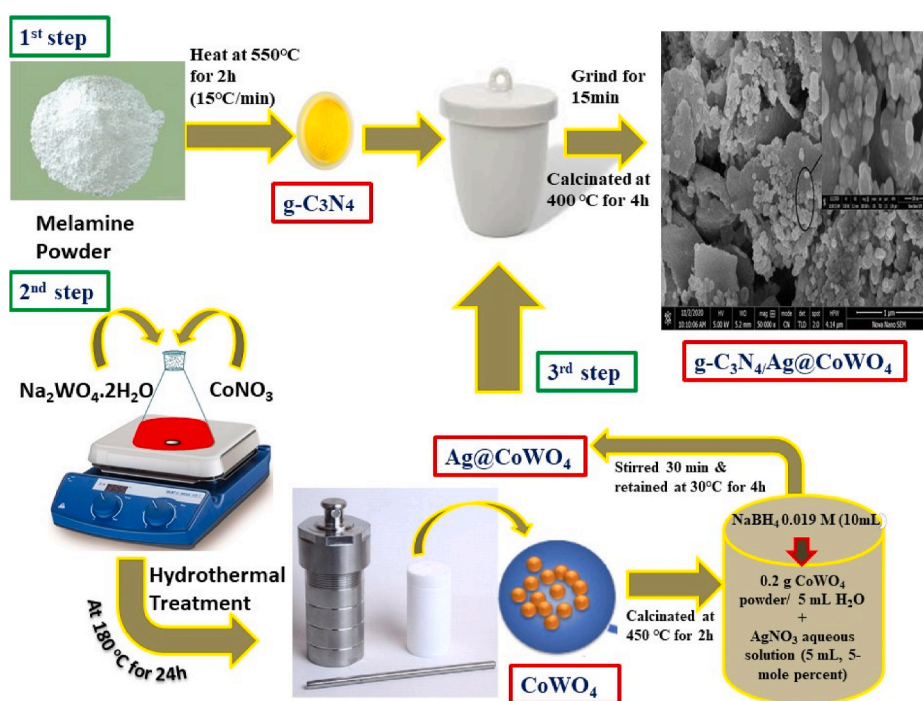

Fig. 1. A schematic representation for the synthesis of g-C₃N₄/Ag@CoWO₄ composite.
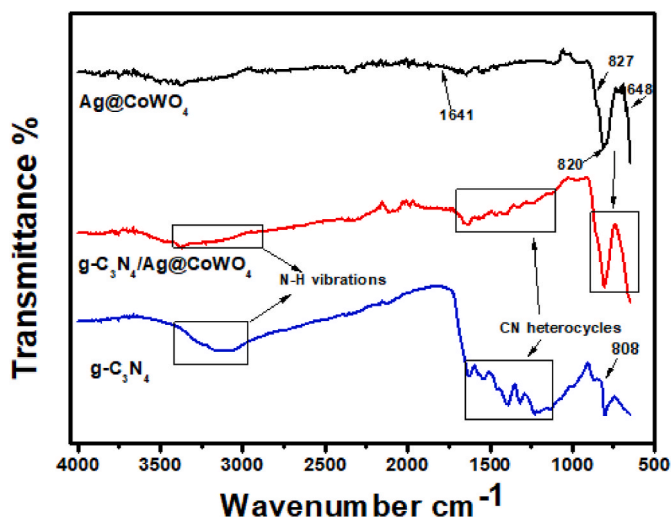
Fig. 2. FTIR analysis of g-C$_3$N$_4$, Ag@CoWO$_4$, and g-C$_3$N$_4$/Ag@CoWO$_4$ composite.

wavenumber range, the characteristic bands of Ag@CoWO$_4$ were observed, which could be due to the existence of W–O–W, W–O, and Co–O bond deformation modes [51]. The band on 820 cm^{-1} was associated with the O–W–O bond [53]. The spectra of, pristine g-C$_3$N$_4$and g-C$_3$N$_4$/Ag@CoWO$_4$ show that the pure g-C$_3$N$_4$ wide band at 3186 cm^{-1} is attributed to the N–H group [54]. Moreover, the band at 807 cm^{-1} is ascribed to tris-triazine units [55]. The distinctive peaks at 827 cm^{-1}, and 648, are linked to CoWO$_4$ [56]. The g-C$_3$N$_4$/Ag@ CoWO$_4$ nanocomposite comprises all peaks of both pure g-C$_3$N$_4$ and Ag@CoWO$_4$ which assure the successful synthesis of the composite photocatalyst.

3.1.2. XRD analysis

The crystallinity, structural analysis, and phase purity of prepared composites were examined by XRD analysis. The crystallographic assembly of g-C$_3$N$_4$, Ag@CoWO$_4$, and as-prepared ternary composite photocatalyst g-C$_3$N$_4$/Ag@CoWO$_4$ was estimated from the XRD pattern presented in Fig. 3. For the pure g-C$_3$N$_4$, a strong peak at 2θ values of 27.6 was seen, referring to the distinctive inter-planner stacking peak (002) (JCPDS No. 50–1512), of an aromatic system as reported previous literature [57]. The CoWO$_4$ nanosphere contains all the diffraction peaks corresponding to the standard JCPDS No. 72–0479 and structure
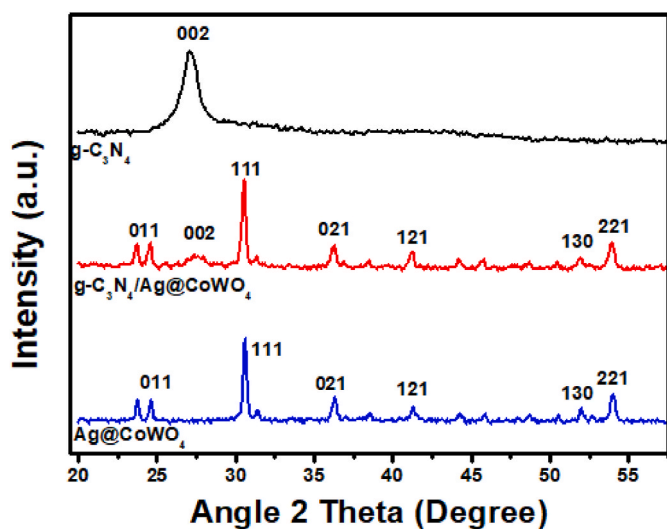

Fig. 3. XRD pattern of g-C$_3$N$_4$, Ag@CoWO$_4$, and g-C$_3$N$_4$/Ag@CoWO$_4$ composite.

is indexed with wolframite monoclinic [58]. All diffraction bands of Ag@CoWO$_4$ were reserved after the coupling of g-C$_3$N$_4$ and with an additional plane of (002) attributed to the aromatic system in g-C$_3$N$_4$. All peaks were narrow and sharp, indicating high crystallinity.

3.1.2.1. Estimation of the size of the nanoparticles (NPs) and the lattice strain using the Williamson-Hall approach. The intensity and width of X-ray diffraction peaks are affected by the change in microstructure of sample [59]. Williamson and Hall improved the Scherrer's formula by identifying that the lattice strain and grain size are the two main sources in broadening of X-ray diffraction peaks at specific temperature. Therefore, according to Williamson and Hall, the full width at half maximum of peak intensity (FWHM = β$_{hkl}$), is the function of both grain size and lattice strain.

$$\beta_{hkl} = \beta_S + \beta_D \qquad (2)$$

$$D_{SH} = \frac{K_{inc}\lambda}{\beta_D Cos\theta_{hkl}} \qquad (3)$$

$$\varepsilon_{W-H} = \frac{\beta_S}{4\, tan\theta_{hkl}} \qquad (4)$$

$$\beta_{hkl} = 4\varepsilon_{W-H}\, tan\theta_{hkl} + \frac{K_{inc}}{D_{W-H} Cos\theta_{hkl}} \qquad (5)$$

$$\beta_{hkl} Cos\theta_{hkl} = 4\varepsilon_{W-H}\, Sin\theta_{hkl} + \frac{K_{inc}\lambda}{D_{W-H}} \qquad (6)$$

here in above Eq (2) the β$_{hkl}$ is the peak broadening, β$_S$ and β$_D$ are the peak width due to lattice strain and grain size respectively. Eq (3) is the standard form of Scherrer's equation. Eq (4) is the Williamson Hall equation considering the β$_S$ strain. Eq (5) is the another form of Eq (2) and so is Eq (6).

By plotting the β$_{hkl}$Cosθ$_{hkl}$ verses 4ε$_{W-H}$ Sinθ$_{hkl}$ on can obtain the size of nanocrystals (D$_{W-H}$) and lattice strain (ε$_{W-H}$) by Williamson Halls method as presented in Figure S-1. The grain size calculated using this approach were 89 nm and 35 nm for Ag@CoWO$_4$, and g-C$_3$N$_4$/Ag@CoWO$_4$ nanocomposite, respectively. Besides the smaller grain size, the lower lattice strain value in case of g-C$_3$N$_4$/Ag@CoWO$_4$ implies lowest lattice imperfection in composite as compared to pristine Ag@CoWO$_4$.

3.1.3. SEM analysis

The surface morphology of g-C$_3$N$_4$, Ag@CoWO$_4$, and g-C$_3$N$_4$/Ag@CoWO$_4$ nanocomposite was investigated by SEM (see Fig. 4). The surface morphology of pristine g-C$_3$N$_4$ displays a sheet-like structure. As-manufactured Ag@CoWO$_4$ shows a higher number of nano-clusters. The nanoparticles nearly spherical in shape were spotted. Also, the agglomeration of high density nanoparticles can be witnessed. No other element was noticed (Fig. 5), verifying the high purity of the synthesized product [60]. The SEM image of g-C$_3$N$_4$/Ag@CoWO$_4$ presents that Ag@CoWO$_4$ nanoparticles are attached to the surface of g-C$_3$N$_4$ nanosheets.

3.1.4. EDX analysis

Fig. 5 shows the element distribution in terms of weight percentage in catalysts.

3.1.5. Bandgap calculation

The optical response of all three catalysts was recorded using a UV–visible spectrophotometer. The spectral scans were recorded from the wavelength from 190 to 900 nm. The absorbance wavelength of all catalysts was observed in the visible region (400–800 nm) providing the photocatalytic activity under the visible region. Therefore, all the experiments were performed under ambient sunlight.

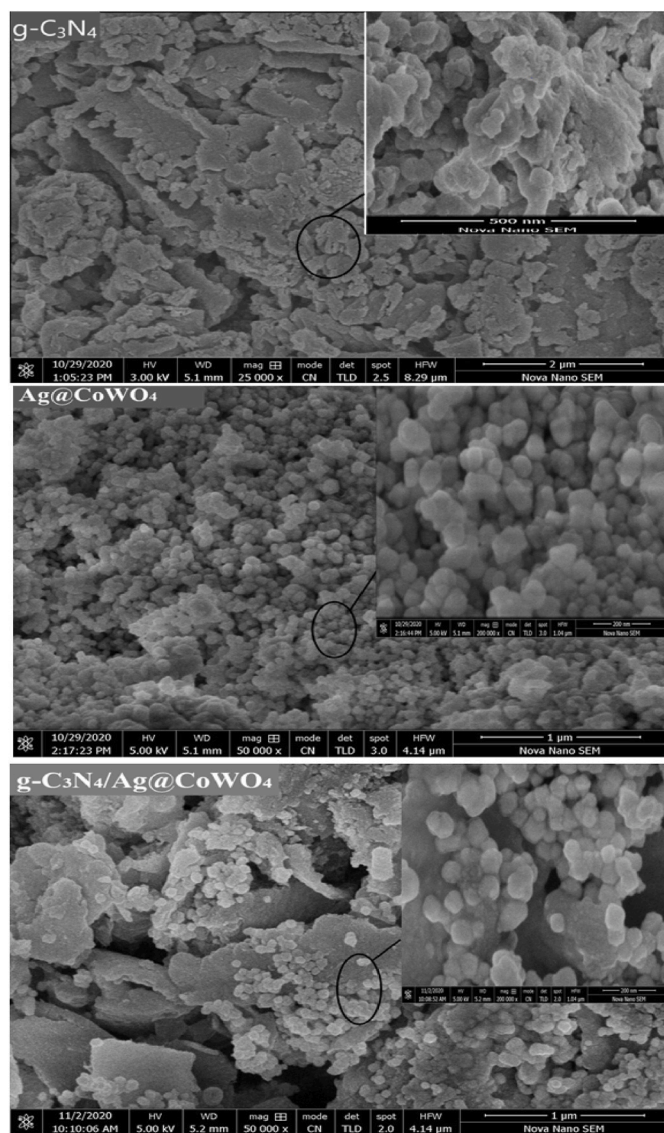The spectral scans and energy band gap (inset) calculations are

Fig. 4. SEM analysis of g-C₃N₄, Ag@CoWO₄, and g-C₃N₄/Ag@CoWO₄ composite.

presented in Fig. 6. The energy band gaps of photocatalysts were estimated using the Tauc plot technique using equation given below;

$$(\alpha h\nu)^n = K \ (h\nu \ - \ E_g) \tag{7}$$

E_g, ν, α, and k is the bandgap energy, light frequency, absorption coefficient, and energy independent constant, respectively. n represents the optical transition of semiconductor materials which is 2 for direct semiconductors [61]. The E_g of the catalysts were obtained from the tangent intercept to x-axis a plot of $(a \ h \ \nu)^2$ versus energy (eV) (inset of Fig. 6). E_g was 2.7 eV for pure g-C₃N₄ [62]. The energy band gap of Ag@CoWO₄ is reported as 2.8 eV [37]. Doping of CoWO₄ with silver reduces the energy band gap [63] up to 2.5 eV as shown in graph. The energy band gap of ternary composite, g-C₃N₄/Ag@CoWO₄ was recorded as 2.3eV. The energy bandgap of ternary composite is smaller than g-C₃N₄ and Ag@CoWO₄ indicating that it might be a potential photocatalyst for the elimination of hazardous organic pollutants under solar/visible light irradiation with excitation energy less as compared to both pristine photocatalysts [43].

3.2. Surface charge determination of catalysts

The surface charge on all three photocatalysts were determined using pH drift method. The detailed process for experimentation has been described in supplementary information. The results of pHpzc (Figure S-1) and effect of solution pH on photocatalytic degradation of RhB are in good agreement with each other, as the best photocatalytic degradation efficiency of catalysts has been observed at pH > pHpzc of catalysts. The RhB is a cationic dye and adsorption is favorable at the solution pH above the point zero charge of catalysts. The pzc of g-C₃N₄, Ag@CoWO₄, and g-C₃N₄/Ag@CoWO₄ were 5.4, 2.3, and 3.7 respectively. The surface of catalyst becomes negative under the solution pH > pHpzc of catalysts therefore adsorption is favored under basic conditions of solution pH.

3.3. Photocatalytic degradation experiments for rhodamine B dye

3.3.1. Influence of pH

The oxidation of organic substances is strongly influenced by pH values both directly and indirectly. The pH of the solution significantly affects the potential of OH radicals, owing to their reciprocal relationship between pH and oxidation potential. Hydroxyl radicals are produced in acidic conditions.

Therefore, the impact of g-C₃N₄/Ag@CoWO₄ on RhB degradation was recorded within the range of pH (2–9) at constant catalysts and oxidant doses. The obtained graph is presented in Fig. 7(a). It was observed that dye degradation was better at higher pH, (pH = 6.0). At lower pH the degradation of pristine Ag@CoWO₄ and composite g-C₃N₄/Ag@CoWO₄ was low which could be due to the competitive effect of cationic dye molecules with the H⁺ ions present in the acidic solution. The results can be effectively correlated with the pHpzc of catalysts. The optimum photocatalytic RhB degradation has been observed at pH > pHpzc of all photocatalysts. This is due to the high adsorption affinity of RhB (cationic dye) under basic solution pH. On the other hand, at pH above then the optimum one, the degradation of RhB decreases gradually the reason for which has been described previously [65,66]. Besides this, the scavenging of hydroxyl radicles under high basic conditions decreases dye degradation.

3.3.2. Influence of catalyst (g-C₃N₄ and Ag@CoWO₄) and composite (g-C₃N₄/Ag@CoWO₄) load

To study the influence of catalysts dose on RhB degradation, the experiments were performed at different concentrations of catalysts (2–60 mg/100 mL) at pH 6. The degradation efficacy of RhB is presented in Fig. 7(b). The results provide the highest value of the response variable at catalysts load of 10 mg/100 mL.

The rhodamine B degradation was considerably affected by catalyst dose. This has been described in terms of the accessibility of active sites on the catalyst surface and effective light penetration into suspension. By increasing the dose of the catalyst, increasing the number of active sites onto the catalyst surface along with the production of free hydroxyl and superoxide radicals increases the rate of degradation. At that time, by increasing the catalyst dosage above the optimized value, the turbidity of suspension increases which reduces the light penetration. Additionally, the catalyst agglomerates and photo-activated volume of suspension decreases. Therefore, the degradation rate is also expected to be decreased at a higher catalyst dose above a balance between dye and catalysts' active site availability.

3.3.3. Effect of oxidant dose

The working of oxidants in oxidative photocatalytic dye degradation follows a famous reaction mechanism in generating reactive species. The disassociation of hydrogen peroxide yields reactive hydroxyl radicles (Eq (8)) and also helps in effective charge separation by accepting the electrons from the conduction band (Eq (9)) [67]:
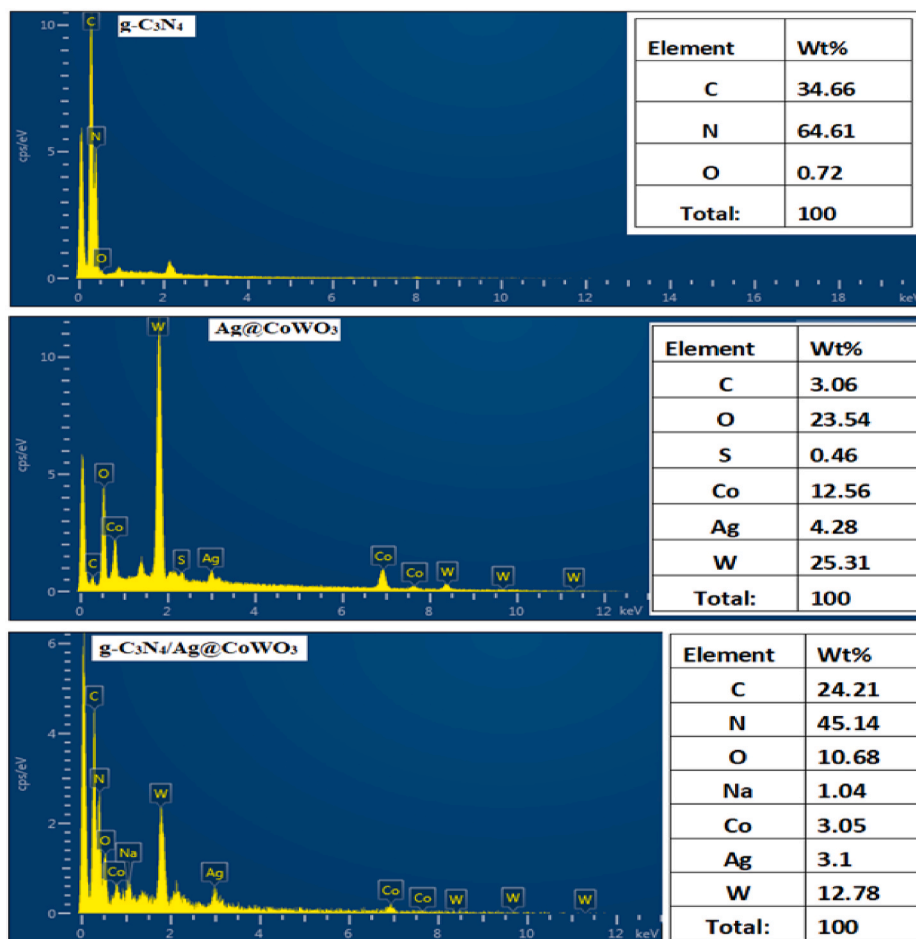
Element	Wt%
C	34.66
N	64.61
O	0.72
Total:	100

Element	Wt%
C	3.06
O	23.54
S	0.46
Co	12.56
Ag	4.28
W	25.31
Total:	100

Element	Wt%
C	24.21
N	45.14
O	10.68
Na	1.04
Co	3.05
Ag	3.1
W	12.78
Total:	100

Fig. 5. EDX analysis of g-C$_3$N$_4$, Ag@CoWO$_4$, and g-C$_3$N$_4$/Ag@CoWO$_4$ composite.

$$H_2O_2 + O_2^{-\cdot} \rightarrow HO^- + HO^\cdot + O_2 \tag{8}$$

$$H_2O_2 + e_{(CB)}^- \rightarrow HO^- + HO^\cdot \tag{9}$$

Owing to the effective contribution of hydrogen peroxide in photocatalytic degradation, the experiments were performed to find out the optimum value from the current study. Some experiments without the addition of oxidant has also been performed and the results are presented in Figure S-2. The results (Fig. 7c) with the addition of hydrogen peroxide presents that a 15 mM concentration of hydrogen peroxide was effective enough for maximum RhB dye degradation. However, further increase in oxidant dose does not found very effective and results in a negative impact on dye degradation [68,69]. The reason for this could be attributed to the hydrogen peroxide radical (HO$_2^\cdot$) formation (the less reactive radical than HO$^\cdot$ radicals). These radicles also act as HO$^\cdot$ scavengers according to Eqs 10 and 11.

$$H_2O_2 + HO^\cdot \rightarrow H_2O + HO_2^\cdot \tag{10}$$

$$HO_2^\cdot + HO^\cdot \rightarrow H_2O + O_2 \tag{11}$$

3.3.4. Influence of RhB load

From an experimental point of view, it is important to examine how initial dye concentration affects the degradation rate. Therefore, a range of RhB dye concentrations (2–16 ppm) was selected for the optimization process at constant oxidant, pH, and catalyst concentrations. The results are presented in Fig. 7(d).

From 2 to 10 ppm of RhB dye concentration the degradation efficiency of the composite photocatalyst was ~100% which decreases gradually with the increase in dye concentration. The high degradation is attributed to the excessive availability of the active site for photocatalysis. as far as the balance between the dye molecules and catalysts actives sites disturbed, the degradation decreases. Besides the unavailability of active sites, the decreased transparency due to high dye concentration is another factor that reduces the degradation process above 10 ppm of RhB dye.

3.3.5. Influence of time

The irradiation time is known as one of the most influencing factors in photocatalytic degradation processes. A rapid increase in degradation was observed in the first 60 min of reaction time after which the degradation rate decreases and reached maximum at ~120 min. At the initial stage, abundant hydroxyl radicals are available, so increasing the rate of degradation. With the time hydroxyl radicals are consumed, so the reaction was progressed at a slower speed. The results are presented in Fig. 7(e).

3.3.6. Stability analysis of catalyst through various runs

To check the reusability of heterogenous nanocomposite photocatalyst the composite (g-C$_3$N$_4$/Ag@CoWO$_4$) was collected after the degradation experiment, washed with distilled water 3–5 times, and dried in air. The composite was reused for stability analysis up to 5 cycles (Fig. 7(f)). The result showed that the activity of nanocomposite does not show a noticeable loss after five recycles for RhB degradation, representing excellent reusability.
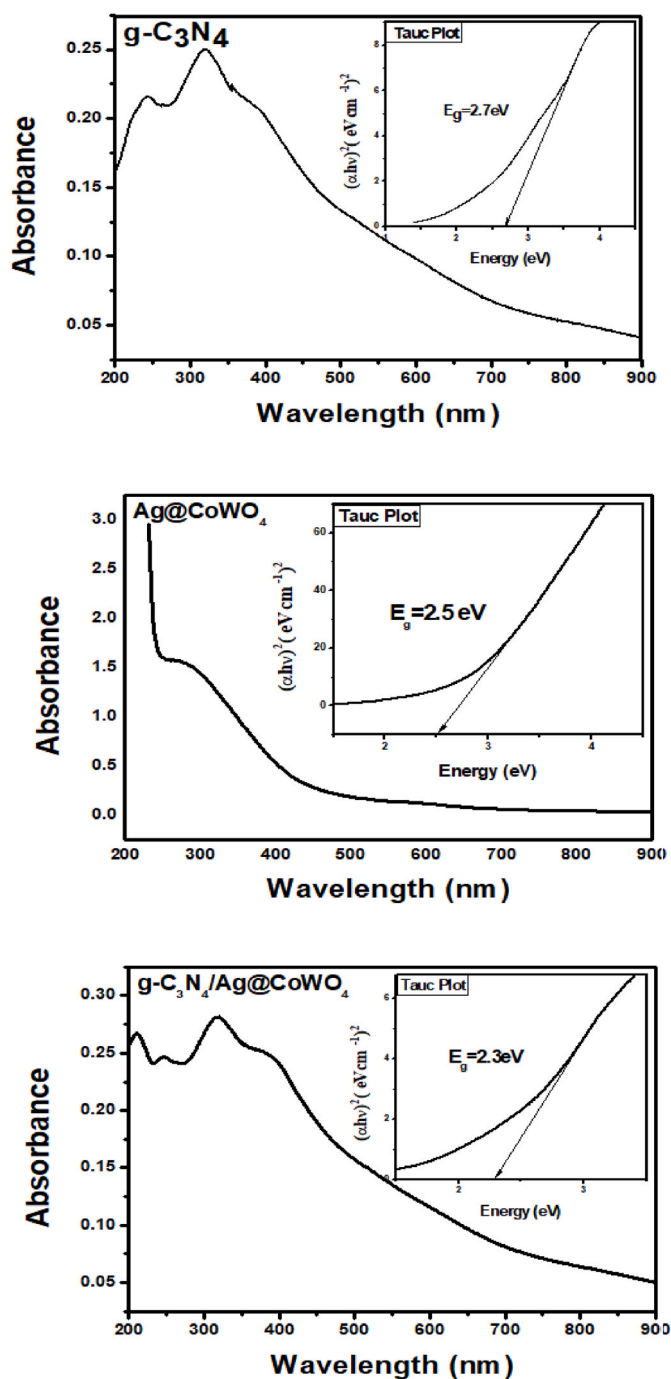
Fig. 6. UV–visible scans of g-C$_3$N$_4$, Ag@CoWO$_4$, and g-C$_3$N$_4$/Ag@CoWO$_4$, inset Tauc plot for energy band gap.

3.4. Radical trapping experiment and proposed photocatalytic degradation mechanism
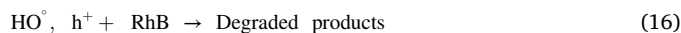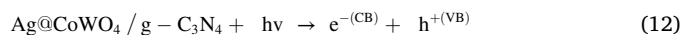
The detail of radical trapping experiment has been described somewhere else [64]. The results are presented in Fig. 8. The results provide clear evidence about the DMSO as key radical scavenger (for OH radical), as the addition of DMSO results dramatic reduction in degradation efficiency from 97% to 35%. Based on radical trapping experiments, the proposed photocatalytic degradation mechanism is given below.

Ag@CoWO$_4$ combined with g-C$_3$N$_4$ is a z-scheme nanocomposite for attaining greater photo-degradation proficiency in visible irradiation, as the heterojunction may improve photo-generated charge separation and

aid to allow greater photocatalytic action. CoWO$_4$ was used as pure and in conjunction with other semiconductors in the photocatalytic processes [37,70]. CoWO$_4$'s CB and VB energies are +0.35 and +3.15 eV, respectively. Therefore, it looks like the photocatalytic efficacy of prepared g–C$_3$N$_4$–centered photocatalyst may be improved by a combination of Ag@CoWO$_4$ with g-C$_3$N$_4$.

Under sunlight the rapid excitation of electrons in g-C$_3$N$_4$/Ag@CoWO$_4$ takes place from the VB to the CB leaving h$^+$ in the VB. The excited electrons from the VB to the conduction band of g-C$_3$N$_4$ are transferred to Ag nanoclusters and trapped efficiently. Meanwhile, the electrons from the conduction band of Ag@CoWO$_4$ transferred to the valance band of g-C$_3$N$_4$ and combined with the partial holes there [20, 71]. The enhanced photocatalytic activity of g-C$_3$N$_4$/Ag@CoWO$_4$ is ascribed to the efficient charge separation. It indicates that g-C$_3$N$_4$/Ag@CoWO$_4$ follows the Z-scheme mechanistic pathway for photocatalytic dye degradation. The g-C$_3$N$_4$ nanocomposite photocatalysis of binary metal oxide particles is believed to follow the Z-scheme pathway [72]. This could promote isolation of the charges and increase the efficiency of photocatalytic degradation. A schematic representation of the z-scheme degradation mechanism is presented in Fig. 8.

Besides, the oxygen molecules may trap the electrons to generate superoxide radicals O$_2^{\circ-}$ and the holes may react with H$_2$O/OH$^-$ to generate the OH radical. These hydroxyl radicals can potentially degrade organic molecules. Some key reaction in photocatalysis is presented below;

$$Ag@CoWO_4 \big/ g-C_3N_4 + \ hv \ \rightarrow \ e^{-(CB)} + \ h^{+(VB)} \tag{12}$$

$$e^- + \ O_2 \rightarrow \ O_2^{\circ-} \tag{13}$$

$$O_2^{\circ-} + H_2O \ \rightarrow \ HO_2^{\circ} + HO^{\circ} \tag{14}$$

$$h^+ + \ H_2O/OH^- - \rightarrow \ HO^{\circ} \tag{15}$$

$$HO^{\circ}, \ h^+ + \ RhB \ \rightarrow \ Degraded \ products \tag{16}$$

3.5. Kinetic modeling of rhodamine B degradation

1st order and 2nd order kinetic reaction models were selected to quantify the photocatalytic degradation of RhB dye. The expressions for the 1st and 2nd order kinetic models are presented in Eqs. (17) and (18) respectively [9,28,65].

$$\ln \ C_o/C_t = -k_1 t \tag{17}$$

$$1/C_t - 1/C_o = k_2 t \tag{18}$$

here, K_1 is the 1st order rate constant while C_0 and Ct are the RhB concentrations at zero and specific reaction time t, respectively [73]. K_1 and K_2 are the rates constant for the 1st and 2nd order kinetic model [74].

Fig. 9(a) presents the graph with a linear relation between ln C$_o$/C$_t$ verses time and Fig. 9(b) presents the graph with a linear relationship of (1/C$_t$-1/C$_o$) versus time. The values of K_1 and K_2 are calculated from the slope of a 1st and 2nd order kinetics as 0.03 and 0.003 min^{-1}, respectively. The R^2 value and rate constant k for RhB degradation are shown in Fig. 9. The R^2 value for 1st order kinetics is best fitted relative to the 2nd kinetics model [27].

3.6. Optimization through RSM

The main objective of the statistical analysis is to examine the influences of certain parameters on the degradation of the rhodamine B dye. Its function is to optimize the parameters. Using central composite design (CCD) under RSM the pH, oxidant dose (H$_2$O$_2$), and composite
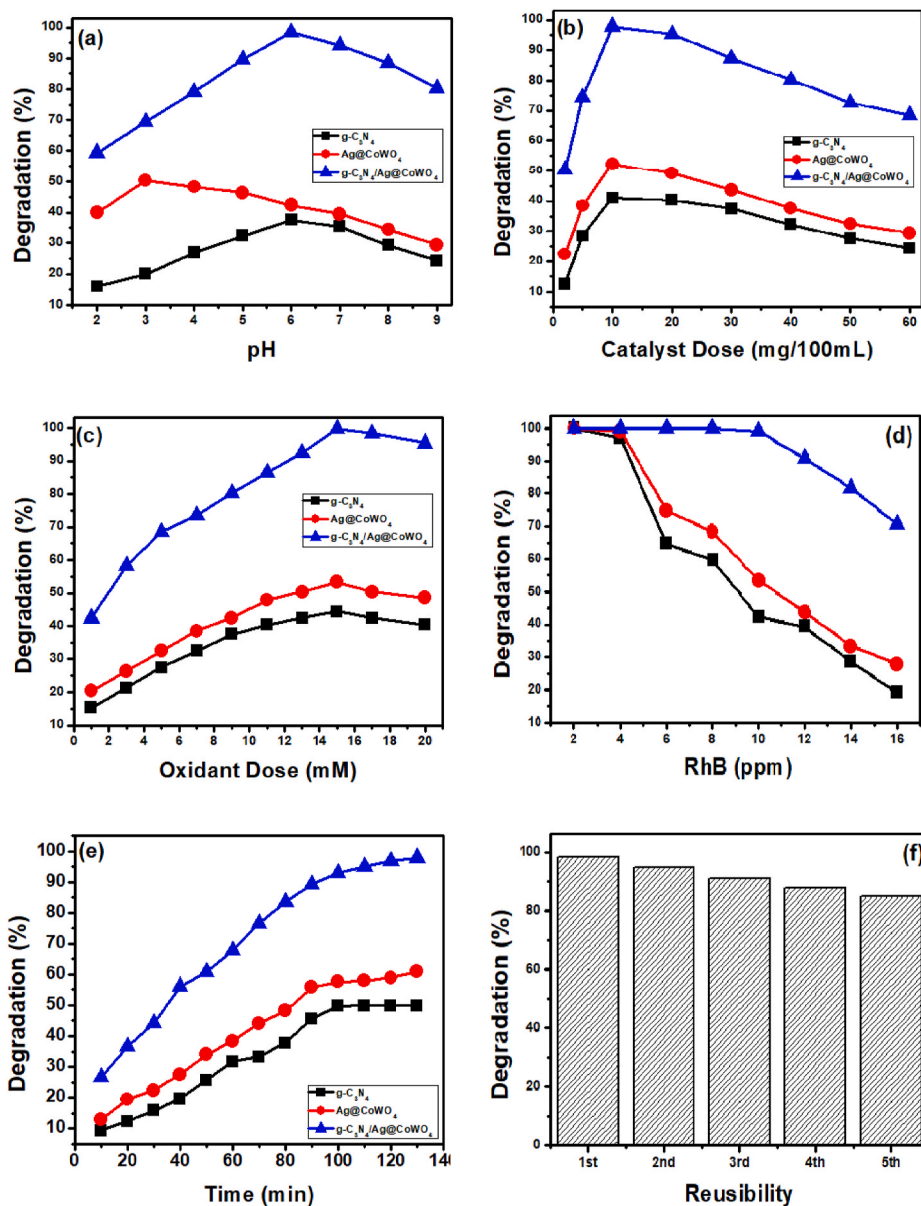
Fig. 7. Effect of different parameters on the degradation of RhB (a) pH, (b) catalysts dose, (c) Oxidant dose, (d) RhB conc. (e) time, and (f) reusability at experimental conditions of pH = 3 for Ag@CoWO4 and 6 for g-C3N4 and g-C3N4/Ag@CoWO4, cat.dose = 0.1 g/L, H2O2 = 15 mM, and reaction time 120 min for each catalyst.
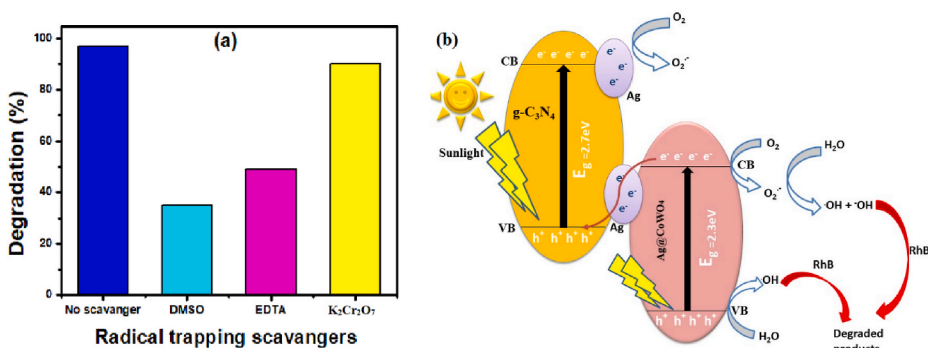

Fig. 8. (a) Radical trapping experiment (b) Proposed photocatalytic dye degradation mechanism of RhB using g-C3N4/Ag@CoWO4 composite.
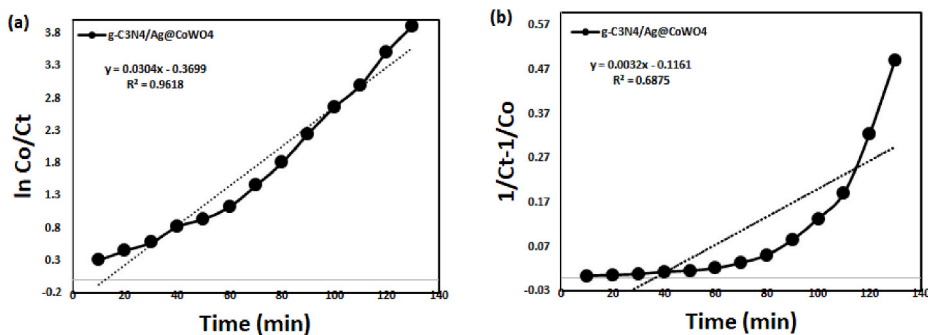
Fig. 9. Kinetic study (a) 1st order kinetic model (b) 2nd order kinetic model for RhB degradation using g-C$_3$N$_4$/Ag@CoWO$_4$ composite.

dose (g-C$_3$N$_4$/Ag@CoWO$_4$) were optimized under visible light at constant dye concentration (10 ppm RhB) and reaction time (120 min). The software Design Expert 7.0.0 was used for RSM. By applying the model, contour and 3-D plots were recorded at a selective range of influencing parameters. The ANOVA model was applied to verify the effect of parameters. It was found that the model was significant. CCD offered 20 trial runs, which were performed and the maximum % degradation was obtained. The experimental matrices for CCD (Figure S-4) is presented in Tables S–1 (supplementary information).

3.6.1. Analysis of variance

The generated model has a high level of significance, as indicated by a fit summary plot. The R^2 value, which is roughly equalized to 1, can be used to determine the importance of model. The efficiency of chosen variables and percent degradation were calculated using this quadratic model. The regression model used second-order polynomial equations to understand the connection between three factors. The quadratic regression model for the degradation of RhB is as follows [27,64]:

dation utilizing gC$_3$N$_4$/Ag@CoWO$_4$ composite are summarized in Table 1. The following is the polynomial quadratic equation in terms of coded factors:

$$\% \text{ Degradation of RhB} = +97.03.02 \times A - 3.00 \times B + 7.29 \times C + 2.61 \times A \times B \\ + 4.53 \times A \times C + 1.82 \times B \times C - 6.88 \times A^2 - 2.97 \times B^2 - 9.25 \times C^2 \tag{20}$$

3.6.1.1. Interpretation. The F-value of Model 15.47 infers that it is a significant model. The F-value 1.43 indicates the Lack of Fit is not significant which is good, the model should be fit. In this case A, B, C, AC, A^2, B^2, C^2 are significant model terms. Values greater than 0.1000 indicate the model terms are not significant.

The properties of the fitted model are shown in Table 2. The "Pred R-Squared" of 0.66 is not as close to the "Adj R-Squared" of 0.87 as one mightnormally expect. Things to consider are model reduction, response tranformation, outliers, etc. The signal-to-noise ratio was measured by "Adeq Precision". A desirable ratio is larger than 4. The 11.699 ratio indicates a satisfactory signal. This model may be used to direct design

$$Y(\% \text{ degradation of RhB using } g-C3N4/Ag@CoWO4) = \beta 0 + \sum_{i=1}^{k} \beta_i X_i + \sum_{i=1}^{k} \beta_{ii} X_i^2 + \sum_{i=1}^{k} \sum_{i \neq j}^{k} \beta_{ij} X_i X_j + \varepsilon \tag{19}$$

The response variable is Y, the coefficient with specified numerical values is bo, and the coefficients relating to quadratic, linear, and interaction effects are bii, bi, and bij, respectively. The number of independent variables is denoted by k, while the random error is denoted by epsilon (e). The ANOVA and regression coefficients for dye degra-

Table 2
Properties of the model.

Std. Dev.	4.64	R-Squared	0.93
Mean	83.98	**Adj R-Squared**	0.87
C.V. %	5.53	**Pred R-Squared**	0.66
PRESS	1108.24	**Adeq Precision**	11.69

Table 1
ANOVA table for RhB degradation using g-C$_3$N$_4$/Ag@CoWO$_4$

| Source	Sum of Squares	df	Mean Square	F Value	p-value Prob > F	
Model	2999.75	9	333.31	15.47	<0.0001	significant
A-pH	124.16	1	124.16	5.76	0.0373	
B-composite dose	123.02	1	123.02	5.71	0.038	
C–H$_2$O$_2$	724.88	1	724.88	33.64	0.0002	
AB	54.44	1	54.44	2.53	0.143	
AC	164.44	1	164.44	7.63	0.02	
BC	26.39	1	26.39	1.22	0.2944	
A^2	681.56	1	681.56	31.63	0.0002	
B^2	127.14	1	127.14	5.9	0.0355	
C^2	1231.95	1	1231.95	57.17	<0.0001	
Residual	215.5	10	21.55			
Lack of Fit	126.89	5	25.38	1.43	0.3516	not significant
Pure Error	88.61	5	17.72			
Cor Total	3215.25	19				
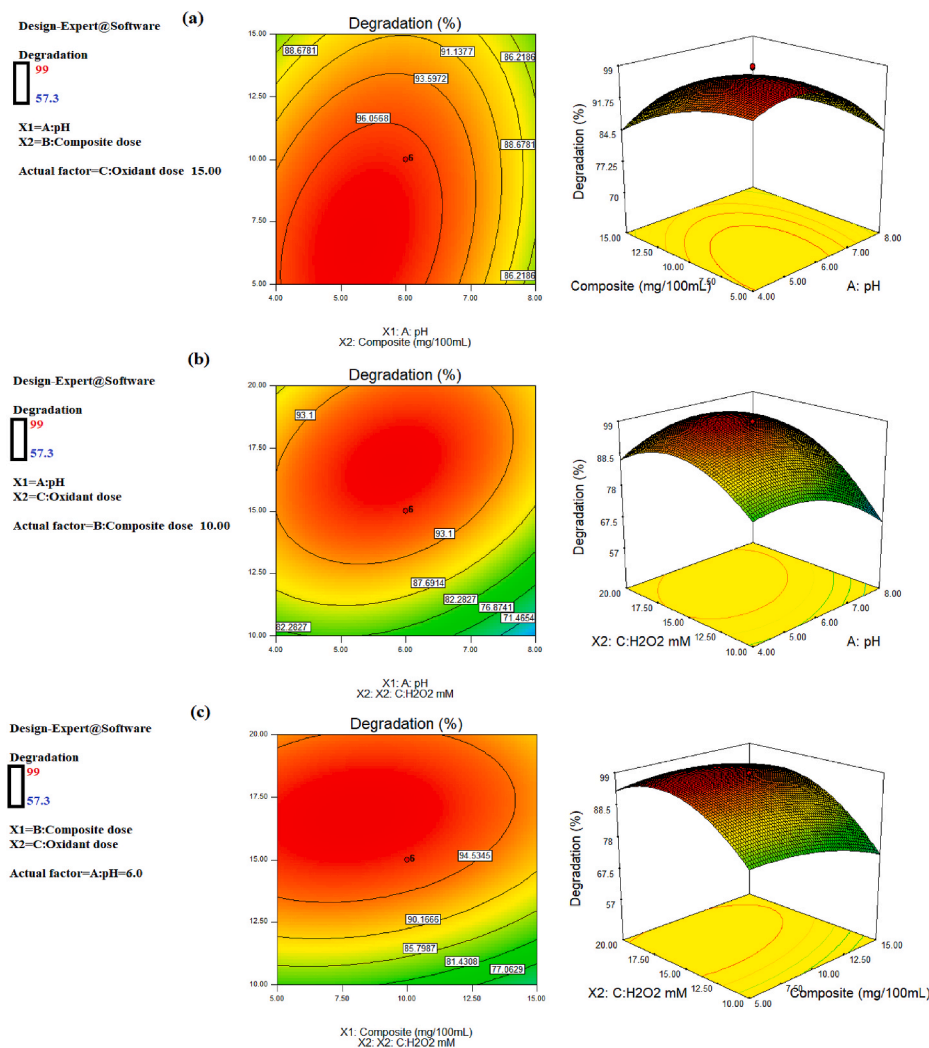
Fig. 10. Response Surface Methodology. L.H.S contour graph, R.H.S 3D graph presenting interaction of independent variables i.e pH, H_2O_2, and g-C_3N_4/Ag@CoWO$_4$ composite.

space.

3.6.2. Optimization and mutual effect of influencing parameters

The parameter pH and catalyst dose show the maximum degradation at pH 6 and catalyst dosage 20 mg (Fig. 10 a). The 3D response surface schemes show the effect of the parameters for the degradation of RhB by the photocatalyst with time. It was seen that reduction in RhB degradation as the concentration of the catalyst increased.

The oxidant dose-effect along with the pH on RhB degradation is presented in Fig. 10(b). The dye degradation increases smoothly with an increase in the H_2O_2 concentration from 3 mM to 15 mM and after that, the degradation starts to stop. The positive effect of the oxidant leads to inhibition of the electron and hole pair rejoining at the surface of the ternary photocatalyst. While at a higher concentration of oxidant dose the hydrogen peroxide also acts as a scavenger for the holes present in the valence band and hydroxyl radicals. On the other side, the pH also showed the same effect that above 6 the degradation started to decrease. This showed that beyond the optimum oxidant concentration and pH values the MB degradation was not enhanced further.

The RhB degradation increased with an increase in the catalyst dose but up to a certain limit, when the composite concentration increased than a specific limit then there will be a decrease in the % of the MB degradation due to the increase in the OH generation and cause undesirable reactions between the oxidant and OH present in the solution.

The contour and 3-D plot showed that with a rise in catalyst amount up to 10 mg and oxidant dose 15 mM, the MB degradation was maximum (i. e., 99%) Fig. 10(c).

By employing the statistical analysis method, the outcome of the optimized parameters was confirmed. The optimized conditions are pH = 6, g-C_3N_4/Ag@CoWO$_4$ = 10 mg/100 mL, and H_2O_2 dose = 15 mM.

4. Conclusion

The novel ternary composite g-C_3N_4/Ag @CoWO$_4$ was fabricated via facile hydrothermal approach for effective oxidative photocatalytic degradation of RhB dye. The g-C_3N_4 and Ag@CoWO$_4$ were also synthesized for the comparison among degradation abilities with the novel ternary composite g-C_3N_4/Ag@CoWO$_4$. All the catalysts were well characterized to analyze the morphological, structural, elemental, and optical properties. The characterization supports the successful fabrication of g-C_3N_4, Ag@CoWO$_4$ nanoparticles, and g–C_3N_4–Ag@CoWO$_4$ composite. This novel combination of Ag@CoWO$_4$ with g-C_3N_4 sheets improves the transfer and separation of photo-induced charge carriers. The reduction in energy band gap values of composite as compared to both pristine catalysts showed effective activity in sunlight at lower excitation energy. The claim has been authenticated from the superior degradation potential of composite. ~99% of RhB dye degradation under ambient sunlight was observed using ternary

g–C$_3$N$_4$–Ag@CoWO$_4$ composite within 120 min. The reusability of catalysts supports reliable results with negligible reduction in degradation performance even after 5 reusability trials. The enhancement in degradation efficiency of g-C$_3$N$_4$/Ag@CoWO$_4$ as compared to pristine g-C$_3$N$_4$ and Ag@CoWO$_4$ was ascribed to the rapid dissociation and facile electron and hole transfer rate due to the improved heterostructure. The projected Z-scheme mechanism of g-C$_3$N$_4$/Ag@CoWO$_4$ suggests the efficient trapping of the reactive species. The novel composite g-C$_3$N$_4$/Ag@CoWO$_4$ can potentially be used for environmental remediation.

Author statement

Hira Ashiq: Investigation, Methodology, Writing—review and editing. Nimra Nadeem: Validation, Writing- Original draft preparation, Revised draft preparation. Asim Mansha: Conceptualization, Software, Revised draft preparation. Javed Iqbal: Formal analysis, Conceptualization, Data curation. Muhammad Yaseen: Resources, Data curation. Muhammad Zahid: Supervision, Project administration, Writing—review and editing. Imran Shahid: Visualization, Writing—review and editing.

Declaration of competing interest

The authors declare that they have no known competing financial interests or personal relationships that could have appeared to influence the work reported in this paper.

Acknowledgments

Appendix A. Supplementary data

Supplementary data to this article can be found online at https://doi.org/10.1016/j.jpcs.2021.110437.

References

[1] C. Dai, Y. Zhou, H. Peng, S. Huang, P. Qin, J. Zhang, Y. Yang, L. Luo, X. Zhang, Current progress in remediation of chlorinated volatile organic compounds: a review, J. Ind. Eng. Chem. 62 (2018) 106–119.

[2] A. Sudhaik, P. Raizada, P. Shandilya, D.Y. Jeong, J.H. Lim, P. Singh, Review on fabrication of graphitic carbon nitride based efficient nanocomposites for photodegradation of aqueous phase organic pollutants, J. Ind. Eng. Chem. 67 (2018) 28–51.

[3] V.J. Thomas, S. Ramaswamy, Application of graphene and graphene compounds for environmental remediation, Sci. Adv. Mater. 8 (2016) 477–500.

[4] M.U. Rahman, U.Y. Qazi, T. Hussain, N. Nadeem, M. Zahid, H.N. Bhatti, I. Shahid, Solar driven photocatalytic degradation potential of novel graphitic carbon nitride based nano zero-valent iron doped bismuth ferrite ternary composite, Opt. Mater. 120 (2021) 111408.

[5] M. Rubab, I.A. Bhatti, N. Nadeem, S.A.R. Shah, M. Yaseen, M.Y. Naz, M. Zahid, Synthesis and photocatalytic degradation of rhodamine B using ternary zeolite/WO3/Fe3O4 composite, Nanotechnology 32 (2021) 345705.

[6] R. Saher, M.A. Hanif, A. Mansha, H.M.A. Javed, M. Zahid, N. Nadeem, G. Mustafa, A. Shaheen, O. Riaz, Sunlight-driven photocatalytic degradation of rhodamine B dye by Ag/FeWO4/g-C3N4 composites, Int. J. Environ. Sci. Technol. 18 (2021) 927–938.

[7] W. Guo, W. Teng, Y. Tang, T. Jiao, Preparation and photocatalytic capacity evaluation of TiO2/BiVO4 nanocrystalline heterojunctions, Sci. Adv. Mater. 8 (2016) 1668–1672.

[8] S.A. Mosavi, A. Ghadi, P. Gharbani, A. Mehrizad, Photocatalytic removal of Methylene Blue using Ag@ CdSe/Zeoilte nanocomposite under visible light irradiation by Response Surface Methodology, Mater. Chem. Phys. 267 (2021) 124696.

[9] N. Nadeem, M. Zahid, H.N. Bhatti, I. Shahid, G. Mustafa, A. Tabasum, Wastewater remediation using coal fly ash nanocomposites, in: Aquananotechnology, Elsevier, 2021, pp. 149–174.

[10] M. Zahid, N. Nadeem, M.A. Hanif, I.A. Bhatti, H.N. Bhatti, G. Mustafa, Metal ferrites and their graphene-based nanocomposites: synthesis, characterization, and applications in wastewater treatment, in: Magnetic Nanostructures, Springer, 2019, pp. 181–212.

[11] M. Zahid, N. Nadeem, N. Tahir, M.I. Majeed, S.A.R. Naqvi, T. Hussain, Hybrid nanomaterials for water purification, in: Multifunctional Hybrid Nanomaterials for Sustainable Agri-Food and Ecosystems, Elsevier, 2020, pp. 155–188.

[12] S. Asadzadeh-Khaneghah, A. Habibi-Yangjeh, M. Abedi, Decoration of carbon dots and AgCl over g-C3N4 nanosheets: novel photocatalysts with substantially improved activity under visible light, Sep. Purif. Technol. 199 (2021) 64–77.

[13] Z. Wu, X. Yuan, H. Wang, Z. Wu, L. Jiang, H. Wang, L. Zhang, Z. Xiao, X. Chen, G. Zeng, Facile synthesis of a novel full-spectrum-responsive Co2. 67S4 nanoparticles for UV-, vis-and NIR-driven photocatalysis, Appl. Catal., B 202 (2017) 104–111.

[14] M. Pirhashemi, A. Habibi-Yangjeh, S.R. Pouran, Review on the criteria anticipated for the fabrication of highly efficient ZnO-based visible-light-driven photocatalysts, J. Ind. Eng. Chem. 62 (2018) 1–25.

[15] D.R. Paul, R. Sharma, P. Panchal, S. Nehra, A. Gupta, A. Sharma, Synthesis, characterization and application of silver doped graphitic carbon nitride as photocatalyst towards visible light photocatalytic hydrogen evolution, Int. J. Hydrogen Energy 45 (44) (2020) 23937–23946.

[16] X. Yan, Z. Wu, C. Huang, K. Liu, W. Shi, Hydrothermal synthesis of CdS/CoWO4 heterojunctions with enhanced visible light properties toward organic pollutants degradation, Ceram. Int. 43 (2017) 5388–5395.

[17] W. Zhu, P. Liu, S. Xiao, W. Wang, D. Zhang, H. Li, Microwave-assisted synthesis of Ag-doped MOFs-like organotitanium polymer with high activity in visible-light driven photocatalytic NO oxidization, Appl. Catal., B 172 (2015) 46–51.

[18] D. Mosconi, D. Mazzier, S. Silvestrini, A. Privitera, C. Marega, L. Franco, A. Moretto, Synthesis and photochemical applications of processable polymers enclosing photoluminescent carbon quantum dots, ACS Nano 9 (2015) 4156–4164.

[19] S.R. Kim, W.K. Jo, Application of a photostable silver-assisted Z-scheme NiTiO3 nanorod/g-C3N4 nanocomposite for efficient hydrogen generation, Int. J. Hydrogen Energy 44 (2019) 801–808.

[20] A. Ataei, A. Mehrizad, K. Zare, Photocatalytic degradation of cefazoline antibiotic using zeolite-supported CdS/CaFe2O4 Z-scheme photocatalyst: optimization and modeling of process by RSM and ANN, J. Mol. Liq. 328 (2021) 115476.

[21] S. Allahveran, A. Mehrizad, Polyaniline/ZnS nanocomposite as a novel photocatalyst for removal of Rhodamine 6G from aqueous media: optimization of influential parameters by response surface methodology and kinetic modeling, J. Mol. Liq. 225 (2017) 339–346.

[22] E.B. Yazdani, A. Mehrizad, Sonochemical preparation and photocatalytic application of Ag-ZnS-MWCNTs composite for the degradation of Rhodamine B under visible light: experimental design and kinetics modeling, J. Mol. Liq. 255 (2018) 102–112.

[23] A. Mehrizad, P. Gharbani, Novel ZnS/carbon nanofiber photocatalyst for degradation of rhodamine 6G: kinetics tracking of operational parameters and development of a kinetic model, Photochem. Photobiol. 93 (2017) 1178–1186.

[24] N. AttariKhasraghi, K. Zare, A. Mehrizad, N. Modirshahla, M.A. Behnajady, Achieving the enhanced photocatalytic degradation of ceftriaxone sodium using CdS-gC 3 N 4 nanocomposite under visible light irradiation: RSM modeling and optimization, J. Inorg. Organomet. Polym. Mater. (2021) 1–11.

[25] S. Kameli, A. Mehrizad, Ultrasound-assisted synthesis of Ag-ZnS/rGO and its utilization in photocatalytic degradation of tetracycline under visible light irradiation, Photochem. Photobiol. 95 (2019) 512–521.

[26] N. Fatima, U.Y. Qazi, A. Mansha, I.A. Bhatti, R. Javaid, Q. Abbas, N. Nadeem, Z. A. Rehan, S. Noreen, M. Zahid, Recent developments for antimicrobial applications of graphene-based polymeric composites: a review, J. Ind. Eng. Chem. 100 (2021) 40–58.

[27] A. Tabasum, M. Alghuthaymi, U.Y. Qazi, I. Shahid, Q. Abbas, R. Javaid, N. Nadeem, M. Zahid, UV-accelerated photocatalytic degradation of pesticide over magnetite and cobalt ferrite decorated graphene oxide composite, Plants 10 (2021) 6.

[28] A. Tabasum, I.A. Bhatti, N. Nadeem, M. Zahid, Z.A. Rehan, T. Hussain, A. Jilani, Degradation of acetamiprid using graphene-oxide-based metal (Mn and Ni) ferrites as Fenton-like photocatalysts, Water Sci. Technol. 81 (2020) 178–189.

[29] P. Bakhtkhosh, A. Mehrizad, Sonochemical synthesis of Sm-doped ZnS nanoparticles for photocatalytic degradation of Direct Blue 14: experimental design by response surface methodology and development of a kinetics model, J. Mol. Liq. 240 (2017) 65–73.

[30] A.G. Khosroshahi, A. Mehrizad, Optimization, kinetics and thermodynamics of photocatalytic degradation of Acid Red 1 by Sm-doped CdS under visible light, J. Mol. Liq. 275 (2019) 629–637.

[31] Y. Liang, R. Shang, J. Lu, W. An, J. Hu, L. Liu, W. Cui, 2D MOFs enriched g-C3N4 nanosheets for highly efficient charge separation and photocatalytic hydrogen evolution from water, Int. J. Hydrogen Energy 44 (2019) 2797–2810.

[32] M. Mousavi, A. Habibi-Yangjeh, Decoration of Fe3O4 and CoWO4 nanoparticles over graphitic carbon nitride: novel visible-light-responsive photocatalysts with exceptional photocatalytic performances, Mater. Res. Bull. 105 (2018) 159–171.

[33] S. Kumar, A. Kumar, A. Bahuguna, V. Sharma, V. Krishnan, Two-dimensional carbon-based nanocomposites for photocatalytic energy generation and environmental remediation applications, Beilstein J. Nanotechnol. 8 (2017) 1571–1600.

[34] P. Martín-Ramos, J. Martín-Gil, R. Dante, F. Vaquero, R. Navarro, J. Fierro, A simple approach to synthesize g-C3N4 with high visible light photoactivity for hydrogen production, Int. J. Hydrogen Energy 40 (2015) 7273–7281.

[35] F. Ding, D. Yang, Z. Tong, Y. Nan, Y. Wang, X. Zou, Z. Jiang, Graphitic carbon nitride-based nanocomposites as visible-light driven photocatalysts for environmental purification, Environ. Sci.: Nano 4 (2017) 1455–1469.

[36] G. Mamba, A. Mishra, Graphitic carbon nitride (g-C$_3$N$_4$) nanocomposites: a new and exciting generation of visible light driven photocatalysts for environmental pollution remediation, Appl. Catal., B 198 (2016) 347–377.

[37] M. Shekofteh-Gohari, A. Habibi-Yangjeh, Fe$_3$O$_4$/ZnO/CoWO$_4$ nanocomposites: novel magnetically separable visible-light-driven photocatalysts with enhanced activity in degradation of different dye pollutants, Ceram. Int. 43 (2017) 3063–3071.

[38] G. Dong, K. Zhao, L. Zhang, Carbon self-doping induced high electronic conductivity and photoreactivity of gC$_3$N$_4$, Chem. Commun. 48 (2012) 6178–6180.

[39] Y. Tang, N. Rong, F. Liu, M. Chu, H. Dong, Y. Zhang, P. Xiao, Enhancement of the photoelectrochemical performance of CuWO$_4$ films for water splitting by hydrogen treatment, Appl. Surf. Sci. 361 (2016) 133–140.

[40] P. Taneja, S. Sharma, A. Umar, S.K. Mehta, A.O. Ibhadon, S.K. Kansal, Visible-light driven photocatalytic degradation of brilliant green dye based on cobalt tungstate (CoWO$_4$) nanoparticles, Mater. Chem. Phys. 211 (2018) 335–342.

[41] R. Bandi, R. Dadigala, B.R. Gangapuram, V. Guttena, Green synthesis of highly fluorescent nitrogen–doped carbon dots from Lantana camara berries for effective detection of lead (II) and bioimaging, J. Photochem. Photobiol., B 178 (2018) 330–338.

[42] A. Maavia, I. Aslam, M. Tanveer, M. Rizwan, M. Iqbal, M. Tahir, H. Hussain, R. Boddula, M. Yousuf, Facile synthesis of g-C$_3$N$_4$/CdWO$_4$ with excellent photocatalytic performance for the degradation of Minocycline, Materials Science for Energy Technologies 2 (2019) 258–266.

[43] M. Ahmed, A. Adam, A. Khan, A. Rehman, M. Qamaruddin, M. Siddiqui, M. Qamar, Improved photoelectrochemical water oxidation under visible light with mesoporous CoWO4, Mater. Lett. 183 (2016) 281–284.

[44] S. Asadzadeh-Khaneghah, A. Habibi-Yangjeh, K. Nakata, Decoration of carbon dots over hydrogen peroxide treated graphitic carbon nitride: exceptional photocatalytic performance in removal of different contaminants under visible light, J. Photochem. Photobiol., A 374 (2019) 161–172.

[45] X. Xing, Y. Gui, G. Zhang, C. Song, CoWO$_4$ nanoparticles prepared by two methods displaying different structures and supercapacitive performances, Electrochim. Acta 157 (2015) 15–22.

[46] S.L. Prabavathi, K. Govindan, K. Saravanakumar, A. Jang, V. Muthuraj, Construction of heterostructure CoWO$_4$/g-C$_3$N$_4$ nanocomposite as an efficient visible-light photocatalyst for norfloxacin degradation, J. Ind. Eng. Chem. 80 (2019) 558–567.

[47] J. Qiao, H. Zhang, G. Li, S. Li, Z. Qu, M. Zhang, J. Wang, Y. Song, Fabrication of a novel Z-scheme SrTiO$_3$/Ag$_2$S/CoWO$_4$ composite and its application in sonocatalytic degradation of tetracyclines, Separ. Purif. Technol. 211 (2019) 843–856.

[48] T.D. Nguyen, C.T. Dinh, T.O. Do, A general procedure to synthesize highly crystalline metal oxide and mixed oxide nanocrystals in aqueous medium and photocatalytic activity of metal/oxide nanohybrids, Nanoscale 3 (2011) 1861–1873.

[49] N. Tian, H. Huang, Y. Zhang, Mixed-calcination synthesis of CdWO$_4$/g-C$_3$N$_4$ heterojunction with enhanced visible-light-driven photocatalytic activity, Appl. Surf. Sci. 358 (2015) 343–349.

[50] L. Liu, D. Ma, H. Zheng, X. Li, M. Cheng, X. Bao, Synthesis and characterization of microporous carbon nitride, Microporous Mesoporous Mater. 110 (2008) 216–222.

[51] F. Lei, B. Yan, H.H. Chen, J.T. Zhao, Molten salt synthesis, characterization, and luminescence properties of Gd2MO6: Eu3+ (M= W, Mo) phosphors, J. Am. Ceram. Soc. 92 (2009) 1262–1267.

[52] X. Wang, K. Maeda, A. Thomas, K. Takanabe, G. Xin, J.M. Carlsson, K. Domen, M. Antonietti, A metal-free polymeric photocatalyst for hydrogen production from water under visible light, Nat. Mater. 8 (2009) 76–80.

[53] F. Shi, J. Meng, Y. Ren, Q. Su, Structure, luminescence and magnetic properties of AgLnW2O8 (Ln= Eu, Gd, Tb and Dy) compounds, J. Phys. Chem. Solid. 59 (1998) 105–110.

[54] D. Lu, P. Fang, W. Wu, J. Ding, L. Jiang, X. Zhao, C. Li, M. Yang, Y. Li, D. Wang, Solvothermal-assisted synthesis of self-assembling TiO 2 nanorods on large graphitic carbon nitride sheets with their anti-recombination in the photocatalytic removal of Cr (VI) and Rhodamine B under visible light irradiation, Nanoscale 9 (2017) 3231–3245.

[55] A. Habibi-Yangjeh, A. Akhundi, Novel ternary g-C3N4/Fe3O4/Ag2CrO4 nanocomposites: magnetically separable and visible-light-driven photocatalysts for degradation of water pollutants, J. Mol. Catal. Chem. 415 (2016) 122–130.

[56] K. Jothivenkatachalam, S. Prabhu, A. Nithya, S. Chandra Mohan, K. Jeganathan, Solar, visible and UV light photocatalytic activity of CoWO4 for the decolourization of methyl orange, Desalination and Water Treatment 54 (2015) 3134–3145.

[57] H. Li, C. Shan, B. Pan, Fe (III)-doped g-C3N4 mediated peroxymonosulfate activation for selective degradation of phenolic compounds via high-valent iron-oxo species, Environ. Sci. Technol. 52 (2018) 2197–2205.

[58] U. Subramanian, S. Naik, R. Tangsali, A. Salker, Upconversion luminescence of cerium doped CoWO4 nanomaterials, J. Lumin. 134 (2013) 464–468.

[59] F. Mushtaq, M. Zahid, A. Mansha, I.A. Bhatti, G. Mustafa, S. Nasir, M. Yaseen, MnFe2O4/coal fly ash nanocomposite: a novel sunlight-active magnetic photocatalyst for dye degradation, Int. J. Environ. Sci. Technol. 17 (2020) 4233–4248.

[60] A. Alborzi, A. Abedini, Synthesis, characterization, and investigation of magnetic and photocatalytic property of cobalt tungstate nanoparticles, J. Mater. Sci. Mater. Electron. 27 (2016) 4057–4061.

[61] M. Rubab, I.A. Bhatti, N. Nadeem, S.A.R. Shah, M. Yaseen, M.Y. Naz, M. Zahid, Synthesis and photocatalytic degradation of rhodamine B using ternary Zeolite/WO3/Fe3O4 composite, Nanotechnology 32 (34) (2021) 345705.

[62] M.-H. Chan, R.-S. Liu, M. Hsiao, Graphitic carbon nitride-based nanocomposites and their biological applications: a review, Nanoscale 11 (2019) 14993–15003.

[63] S.F. Ahmed, M.-W. Moon, K.-R. Lee, Effect of silver doping on optical property of diamond like carbon films, Thin Solid Films 517 (2009) 4035–4038.

[64] N. Nadeem, Q. Abbas, M. Yaseen, A. Jilani, M. Zahid, J. Iqbal, A. Murtaza, M. Janczarek, T. Jesionowski, Coal fly ash-based copper ferrite nanocomposites as potential heterogeneous photocatalysts for wastewater remediation, Appl. Surf. Sci. 565 (2021) 150542.

[65] N. Nadeem, M. Zahid, A. Tabasum, A. Mansha, A. Jilani, I.A. Bhatti, H.N. Bhatti, Degradation of reactive dye using heterogeneous photo-Fenton catalysts: ZnFe2O4 and GO-ZnFe2O4 composite, Mater. Res. Express 7 (2020), 015519.

[66] A. Tabasum, M. Alghuthaymi, U.Y. Qazi, I. Shahid, Q. Abbas, R. Javaid, N. Nadeem, M. Zahid, UV-accelerated photocatalytic degradation of pesticide over magnetite and cobalt ferrite decorated graphene oxide composite, Plants 10 (2021) 6.

[67] W. Chu, W.K. Choy, T.Y. So, The effect of solution pH and peroxide in the TiO2-induced photocatalysis of chlorinated aniline, J. Hazard Mater. 141 (2007) 86–91.

[68] A. Enesca, L. Isac, L. Andronic, D. Perniu, A. Duta, Tuning SnO2–TiO2 tandem systems for dyes mineralization, Appl. Catal., B 147 (2014) 175–184.

[69] M. Visa, C. Bogatu, A. Duta, Tungsten oxide – fly ash oxide composites in adsorption and photocatalysis, J. Hazard Mater. 289 (2015) 244–256.

[70] K. Adib, M. Rahimi-Nasrabadi, Z. Rezvani, S.M. Pourmortazavi, F. Ahmadi, H. R. Naderi, M.R. Ganjali, Facile chemical synthesis of cobalt tungstates nanoparticles as high performance supercapacitor, J. Mater. Sci. Mater. Electron. 27 (2016) 4541–4550.

[71] M. Xue, M. Bao, X. Li, L. Qin, S. Han, S.-Z. Kang, A novel pathway toward efficient and stable C3N4-based photocatalyst for light driven H2 evolution: the synergistic effect between Pt and CoWO4, Int. J. Hydrogen Energy 44 (2019) 28113–28122.

[72] J. Fu, Q. Xu, J. Low, C. Jiang, J. Yu, Ultrathin 2D/2D WO3/g-C3N4 step-scheme H2-production photocatalyst, Appl. Catal., B 243 (2019) 556–565.

[73] T. Fan, C. Chen, Z. Tang, Y. Ni, C. Lu, Synthesis and characterization of g-C$_3$N$_4$/BiFeO$_3$ composites with an enhanced visible light photocatalytic activity, Mater. Sci. Semicond. Process. 40 (2015) 439–445.

[74] Y.-S. Ho, Review of second-order models for adsorption systems, J. Hazard Mater. 136 (2006) 681–689.